ACS APPLIED MATERIALS & INTERFACES

Research Article

www.acsami.org

Processing and Characterization of $SrTiO_3$–TiO_2 Nanoparticle–Nanotube Heterostructures on Titanium for Biomedical Applications

Yu Wang,[†] Dongmei Zhang,[†] Cuie Wen,[‡] and Yuncang Li*[,‡]

[†]Institute for Frontier Materials, Deakin University, Geelong, Victoria 3217, Australia

[‡]School of Aerospace, Mechanical and Manufacturing Engineering, RMIT University, Melbourne, Victoria 3000, Australia

ABSTRACT: Surface properties such as physicochemical characteristics and topographical parameters of biomaterials, essentially determining the interaction between the biological cells and the biomaterial, are important considerations in the design of implant materials. In this study, a layer of $SrTiO_3$–TiO_2 nanoparticle–nanotube heterostructures on titanium has been fabricated via anodization combined with a hydrothermal process. Titanium was anodized to create a layer of titania (TiO_2) nanotubes (TNTs), which was then decorated with a layer of $SrTiO_3$ nanoparticles via hydrothermal processing. $SrTiO_3$–TiO_2 heterostructures with high and low volume fraction of $SrTiO_3$ nanoparticle (denoted by 6.3-Sr/TNTs and 1.4-Sr/TNTs) were achieved by using a hydrothermal processing time of 12 and 3 h, respectively. The in vitro biocompatibility of the $SrTiO_3$–TiO_2 heterostructures was assessed by using osteoblast cells (SaOS2). Our results indicated that the $SrTiO_3$–TiO_2 heterostructures with different volume fractions of $SrTiO_3$ nanoparticles exhibited different Sr ion release in cell culture media and different surface energies. An appropriate volume fraction of $SrTiO_3$ in the heterostructures stimulated the secretion of cell filopodia, leading to enhanced biocompatibility in terms of cell attachment, anchoring, and proliferation on the heterostructure surface.

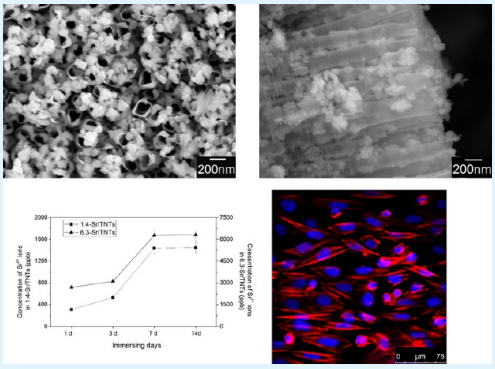

KEYWORDS: *TiO_2 nanotube, $SrTiO_3$–TiO_2 nanoparticle–nanotube heterostructure, surface energy, biocompatibility, SaOS2 cell*

1. INTRODUCTION

As life span in populations increases worldwide, degenerative diseases have become a prevalent, critical issue for an aging population. Organs, joints, and other critical body parts degenerate, and modern medical science offers transplant and implant solutions. However, despite the success of surgical implants, such as hip replacements, the artificial bone substitutes used in these procedures still do not satisfy the demands of a sustainable health care system. Titanium (Ti) and some of its alloys are widely used in biomedical applications, such as dental and orthopedic implants, due to their excellent biocompatibility.[1,2] It is estimated that 20–25% of people having a hip replacement today will eventually require a revision after 20 to 25 years of use in the human body because of the unsatisfactory osseointegration and biocompatibility.[2] Therefore, new implant materials with improved biocompatibility through advanced surface design and modification are highly desirable. Surface modification on Ti substrates was necessary to improve the bioactivity of Ti, which restricted the osseointegration between osteoblast cells and the implants.[3,4] A nanostructured Ti surface was fabricated to stimulate the attachment and proliferation of osteoblast cells.[5] Anodic TiO_2 nanotubular layers were expected to be promising biomaterial surfaces with outstanding in vitro biocompatibility[6] and large specific surface area.[7] Furthermore, TiO_2 nanotubes could be decorated and modified for drug delivery.[8−10] There were a few studies investigating the decorating of TiO_2 nanotubes with $SrTiO_3$,[11−14] Fe_3O_4,[7] and Ag[15,16] nanoparticles for biomedical applications.

Strontium (Sr) is an essential trace element in the body to promote the proliferation of osteoblast cells,[14,17−19] and it is beneficial for calcium deposition for new bone formation.[20] However, it is reported that high concentration of Sr demonstrated adverse effects.[17,21,21] Hydroxyapatite with a doping of high concentration of Sr (>10 at%) demonstrated cytotoxic to L929 cells (a fibroblastic cell line), but a doping of low concentration of Sr (1 and 5 at%) was demonstrated biocompatible.[19] The proliferation of MG-63 cells and alkaline phosphatase activities (ALP) were inhibited on Sr-HA composite with a Sr concentration of 40%.[17]

In this study, strontium titanate–titania ($SrTiO_3$–TiO_2) nanoparticle–nanotube heterostructures on titanium were fabricated via anodization combined with a hydrothermal process. Titanium was anodized to create a surface layer of TiO_2 nanotubes (TNTs), and then a hydrothermal process was carried out to decorate a layer of $SrTiO_3$ nanoparticles with high and low concentrations of Sr. The cell behaviors on the $SrTiO_3$–TiO_2 heterostructures with different contents of Sr in terms of biocompatibility, cell attachment, adhesion, and

Received: May 18, 2015
Accepted: July 2, 2015
Published: July 2, 2015

ACS Publications © 2015 American Chemical Society

DOI: 10.1021/acsami.5b04304
ACS Appl. Mater. Interfaces 2015, 7, 16018−16026

proliferation were investigated using osteoblast-like (SaOS2) cells.

2. EXPERIMENTAL SECTION

2.1. Anodization of TiO_2 nanotubes. Pure Ti plates (10 mm × 10 mm × 1 mm, purity >99.7%) were used as the starting material. Prior to anodization, the Ti plates were progressively sonicated in distilled water, ethanol and acetone for 10 min. The electrolyte was prepared with 0.3 wt % ammonium fluoride (Sigma-Aldrich, Australia), 10 wt % distilled water and ethylene glycol (Sigma-Aldrich, Australia). Titania (TiO_2) nanotubes (TNTs) were anodized at 30 V for 4 h.[22] As-anodized TiO_2 nanotubes were then annealed at 500 °C in air with heating and cooling rate of 1 °C/min.

2.2. Hydrothermal synthesis of $SrTiO_3$−TiO_2 heterostructures. A hydrothermal method was used to synthesize the strontium-titanate-titania ($SrTiO_3$−TiO_2) nanoparticle−nanotube heterostructures. The strontium (Sr) concentration in the heterostructures can be controlled through adjusting the hydrothermal synthesis time. In this study, two kinds of $SrTiO_3$−TiO_2 heterostructures were prepared: one with a saturated Sr ion concentration released in the media of 6.3 mg/L (referred as 6.3-Sr/TNTs) and the other with a saturated Sr ion concentration released in the media of 1.4 mg/L (referred as 1.4-Sr/TNTs). Annealed TNTs samples on the Ti substitute plates were placed in 10 mL of 0.02 M $Sr(OH)_2$ (Sigma-Aldrich, Australia) solution in an autoclave. The autoclave was placed in an oven at 120 °C and kept for 12 and 3 h to obtain 6.3-Sr/TNTs and 1.4-Sr/TNTs samples, respectively. The samples were finally cleaned with 0.02 M hydrochloric acid (HCl) and distilled water for 2 min each step.

2.3. Characterization of the SrTiO3-TiO_2 heterostructures. The phase structures of TNTs, 1.4-Sr/TNTs, and 6.3-Sr/TNTs samples were characterized by X-ray diffraction (XRD, X'pert pro-MPD, PANalytical, The Netherlands) with Cu K_α incident radiation at 40 kV and 30 mA. Morphologies and elemental analysis of the samples were carried out by using scanning electron microscopy (SEM, Supra 55 VP, Zeiss, Germany) equipped with energy dispersive X-ray spectroscopy (EDX, Oxford, UK) and transmission electron microscopy with EDX analysis (TEM, JEOL-2100F, Japan). The surface profile and the absolute roughness (R_a) were analyzed using atomic force microscopy (AFM, Cypher, Asylum Research).

A contact angle tester (KSV Cam 101, KSV Instruments, Inc., Finland) was used to measure the hydrophilicity of the samples. To avoid the effects of temperature and humidity, all samples were stored in the testing room for 24 h prior to the testing. Ultrapure distilled water and ethylene glycol drops with a volume of 5 μL were delivered onto the specimen surface using a syringe. The contact angel was tested after 10 s and repeated 5 times for each group of samples. The surface energy was calculated according to the Owens−Wendt (OW) method given by[23,24]

$$(1 + \cos\theta)\gamma_L = 2\left(\sqrt{\gamma_L^d \gamma_S^d} + \sqrt{\gamma_L^p \gamma_S^p}\right) \quad (1)$$

$$\gamma_S = \gamma_S^d + \gamma_S^p \quad (2)$$

where θ is the contact angle; γ is the surface evergy; the subscripts L and S stand for liquid and solid, respectively; the supscripts d and p represent the dispersive component and polar component. The surface energy, dispersive component, and polar component for distilled water are 72.8 mJ/m^2, 21.8 mJ/m^2, and 51.0 mJ/m^2, and those for ethylene glycol are 48.0 mJ/m^2, 29.0 mJ/m^2, and 19.0 mJ/m^2, respectively.[22]

2.4. Biocompatibility assessment for the $SrTiO_3$−TiO_2 heterostructures. All samples for cell culture were sterilized at 180 °C for 3 h in a muffle furnace. Osteoblast-like cells (SaOS2), a human osteosarcoma cell line with osteoblast properties were used for the in vitro biocompatibility assessment (Barwon Biomedical Research, Geelong Hospital, Victoria, Australia). SaOS2 were seeded on the surface of samples with a cell density of 1 × 10^4 cells per well. Cell proliferation and viability were assessed by using MTS assay. The morphology of cells was observed after culturing for 1 and 5 d using a confocal microscopy (Leica SP5, Leica Microsystems, Germany) and SEM. The cell-seeded samples were fixed with paraformaldehyde, then permeabilized with triton-X 100 in phosphate-buffered saline (PBS, Sigma-Aldrich, Australia) for 10 min at room temperature. The samples were then cultured with 1% phalloidin and 40−6-diamidino-2-phenylindole for 40 min at ambient temperature and washed with three washes by using PBS solution. The prepared samples were stored at 4 °C in PBS until required for the observation by using a confocal microscopy. After that, cells on the samples were dehydrated by immersing in buffer solution with the ethanol concentrations increased from 60 to 100% progresively every 10 min. Then chemical drying was performed with hexamethyldisilazane (HMDS, Sigma-Aldrich, Australia) for 10 min. A gold layer was deposited on the samples prior to SEM observation.

The ion release of the Sr/TNTs heterostructures during immersion in cell culture media was assessed by measuring the Sr^{2+} ion concentrations using inductively coupled plasma mass spectrometry (ICP-MS, Agilent 7700X, US). The Sr/TNTs samples were immersed in 10 mL cell culture media at 37 °C for 1 d, 3 d, 7 and 14 d. The liquid was withdrawn and filtered through a 0.22-μm filter (Falcon, BD Biosciences, San Jose, CA, USA). The Sr^{2+} ions release from the samples were measured.

In all cases, the significant difference in the data was evaluated with one-way analysis ofvariance, and the statistical difference was considered to be significant at $p < 0.05$.

3. RESULTS

3.1. XRD patterns of $SrTiO_3$−TiO_2 heterostructure nanotubes. The XRD patterns of the TiO_2 nanotubes and the $SrTiO_3$−TiO_2 nanoparticle−nanotube heterostructures on Ti substitute are shown in Figure 1. It can be seen that the main

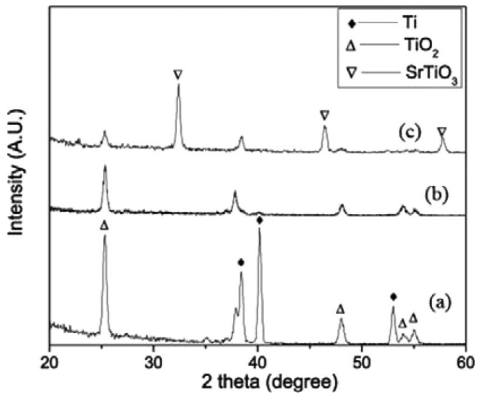

Figure 1. XRD patterns: (a) TNTs, (b) 1.4-Sr/TNTs, and (c) 6.3-Sr/TNTs.

phases of the annealed TNTs (Figure 1a) were Ti (JCPDS No. 1-1197) and anatase TiO_2 (JCPDS No. 2-387). The 1.4-Sr/TNTs (Figure 1b) exhibited peaks of anatase TiO_2 with decreased intensities compared to those of the annealed TNTs. The 6.3-Sr/TNTs (Figure 1c) exhibited peaks for the phases of $SrTiO_3$ (JCPDS No. 1-1018) and anatase TiO_2 with further decreased intensities. The XRD patterns confirmed the synthesis of $SrTiO_3$ in the 6.3-Sr/TNTs which was hydrothermal treated for 12 h, while $SrTiO_3$ was hardly detectable in the 1.4-Sr/TNTs sample due to its low volume fraction resulted from the short hydrothermal processing time of 3 h.

3.2. Surface characteristics of $SrTiO_3$−TiO_2 heterostructures. The surface roughness of the four kinds of samples, including pure Ti, annealed TNTs, 1.4-Sr/TNTs, and 6.3-Sr/TNTs, was measured using AFM, and the roughness (Ra) values are shown in Figure 2. It can be seen that the pure Ti showed the highest roughness of 108.1 nm and the TNTs the lowest roughness of 60.5 nm among the four kinds of

DOI: 10.1021/acsami.5b04304
ACS Appl. Mater. Interfaces 2015, 7, 16018−16026

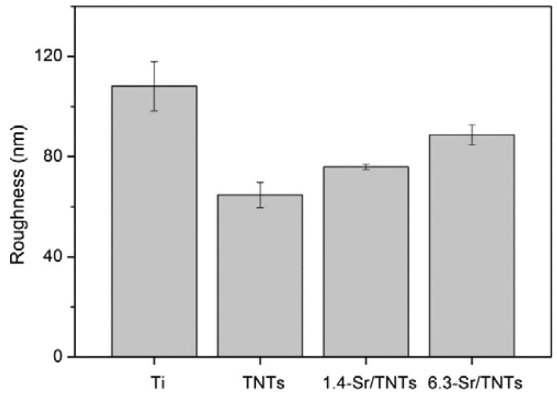

Figure 2. Surface roughness of Ti, TNTs, 1.4-Sr/TNTs, and 6.3-Sr/TNTs.

sample surfaces. The roughness of 6.3-Sr/TNTs was 88.7 nm, which is higher than that of 1.4-Sr/TNTs, 75.9 nm.

The droplet images of distilled water on the surface of Ti, TNTs, 1.4-Sr/TNTs, and 6.3-Sr/TNTs are shown in Figure 3.

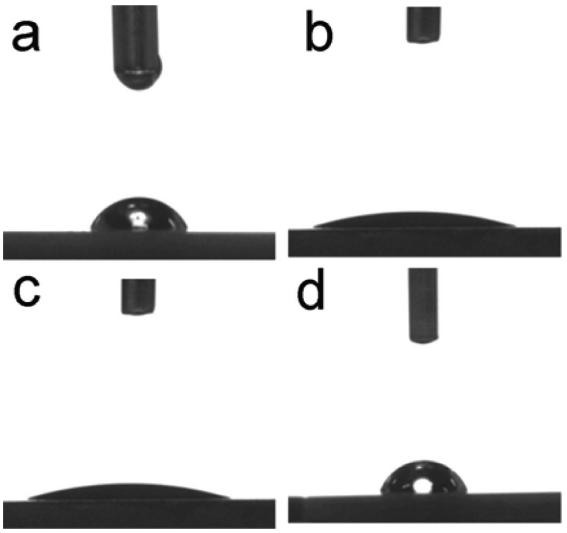

Figure 3. Droplet images of distilled water on the surface of (a) pure Ti, (b) TNTs, (c) 1.4-Sr/TNTs, and (d) 6.3-Sr/TNTs.

The contact angles between the droplet of distilled water and the surface of 1.4-Sr/TNTs and 6.3-Sr/TNTs were 14.2° and 43.7°, respectively. The surface energies of the four samples of Ti, TNTs, 1.4-Sr/TNTs, and 6.3-Sr/TNTs were calculated and listed in Table 1. It can be seen that the Ti without any surface treatment exhibited the lowest surface energy of 26.78 mJ/m^2 and the 1.4-Sr/TNTs showed the highest surface energy of 65.60 mJ/m^2.

3.3. Morphology of $SrTiO_3$–TiO_2 heterostructures. The morphologies of the $SrTiO_3$–TiO_2 nanoparticle–nanotube heterostructures on the Ti substitute are shown in Figure 4. It can be seen that the $SrTiO_3$ nanoparticles were decorated on the walls of TiO_2 nanotubes in the 1.4-Sr/TNTs (Figure 4a), and almost a full layer of $SrTiO_3$ nanoparticles with particle size around 50 nm was aggregated on the 6.3-Sr/TNTs (Figure 4b). The $SrTiO_3$ nanoparticles with a cubic shape were further confirmed by high resolution TEM image (Figure 4c). As shown in the EDX result, the elemental compositions of the $SrTiO_3$–TiO_2 samples are strontium, titanium, and oxygen; the copper peaks are attributed to the TEM grid.

Table 1. Surface Energies of Ti, TNTs, 1.4-Sr/TNTs, and 6.3-Sr/TNTs

Samples	γ^d (mJ/m^2)	γ^p (mJ/m^2)	γ (mJ/m^2)
Ti	9.78 (±0.07)	17.00 (±0.16)	26.78 (±0.21)
TNTs	10.11 (±0.34)	45.41 (±0.48)	55.53 (±0.26)
1.4-Sr/TNTs	6.09 (±0.09)	59.51 (±0.91)	65.60 (±0.91)
6.3-Sr/TNTs	22.54 (±0.91)	19.04 (±0.46)	41.59 (±0.99)

3.4. Release of Sr^{2+} ions from $SrTiO_3$–TiO_2 heterostructures. Figure 5 shows the concentrations of Sr^{2+} ions in cell culture media released from 1.4-Sr/TNTs and 6.3-Sr/TNTs. The concentrations of Sr^{2+} ions exhibited a significant increase in the period from 1 to 7 d; then, no obvious change was observed on the concentrations of Sr^{2+} ions for both samples from 14 to 21 d. The maximum concentrations of Sr^{2+} ions were 1449 ± 124 and 6312 ± 271 ppb after immersing in cell culture media for 14 d for 1.4-Sr/TNTs and 6.3-Sr/TNTs, respectively. The released concentrations of Sr^{2+} ions from 6.3-Sr/TNTs were significantly higher than that of 1.4-Sr/TNTs at any period of immersion.

3.5. Proliferation and adhesion of SaOS2 on $SrTiO_3$–TiO_2 heterostructural surfaces. Figure 6 presents the cell proliferation on the four kinds of surfaces, including Ti, TNTs, 1.4-Sr/TNTs, and 6.3-Sr/TNTs after culturing for 7 and 14 d. It can be seen that 1.4-Sr/TNTs demonstrated the highest cell proliferation and 6.3-Sr/TNTs showed the lowest cell proliferation among all the samples. It is also noted that the number of SaOS2 cells was higher on TiO_2 nanotubes than on bare Ti.

After cell culture for 1 and 5 d, the confocal images of the cell morphologies on Ti, TNTs, 1.4-Sr/TNTs, and 6.3-Sr/TNTs are shown in Figure 7. It can be seen that 1.4-Sr/TNTs displayed the greatest cell numbers among all the samples after cell culture for 1 d. Also, the cell numbers on Ti, TNTs, and 1.4-Sr/TNTs after cell culture for 5 d were significantly increased compared to those after cell culture for 1 d, while the cell numbers on 6.3-Sr/TNTs almost maintained the same, as the cell culture time increased from 1 to 5 d.

The SEM images of SaOS2 cells on Ti, TNTs, 1.4-Sr/TNT$_S$, and 6.3-Sr/TNTs after cell culture for 5 d are shown in Figure 8. It can be seen that the number of cells attached onto the 6.3-Sr/TNTs surface was much lower than those on the other sample surfaces. Furthermore, the SaOS2 cells on the 6.3-Sr/TNTs surface displayed a round and shrinking shape without stretching long filopodia, suggesting that the cells were not growing and spreading healthily (Figure 8d). It is also noted that the cells on 1.4-Sr/TNTs (Figure 8c) and TNTs (Figure 8b) exhibited an elongated shape with plenty of long filopodia stretching on the nanoheterostructural and nanotubular surfaces. The SaOS2 cells on Ti (Figure 8a) showed limited cell number and less stretching filopodia compared to those on 1.4-Sr/TNTs and TNTs, but the cells were healthier than those on 6.3-Sr/TNTs.

4. DISCUSSION

4.1. Loading and releasing mechanism of Sr^{2+} ions from $SrTiO_3$–TiO_2 nanoparticle–nanotube heterostructures. In this study, the $SrTiO_3$–TiO_2 composites displayed a heterostructure with secondary $SrTiO_3$ nanoparticles grafted on TiO_2 nanotubes. The $SrTiO_3$ nanoparticles exhibited very uniform cubic shapes, and the TiO_2 nanotubes were highly

DOI: 10.1021/acsami.5b04304
ACS Appl. Mater. Interfaces 2015, 7, 16018–16026

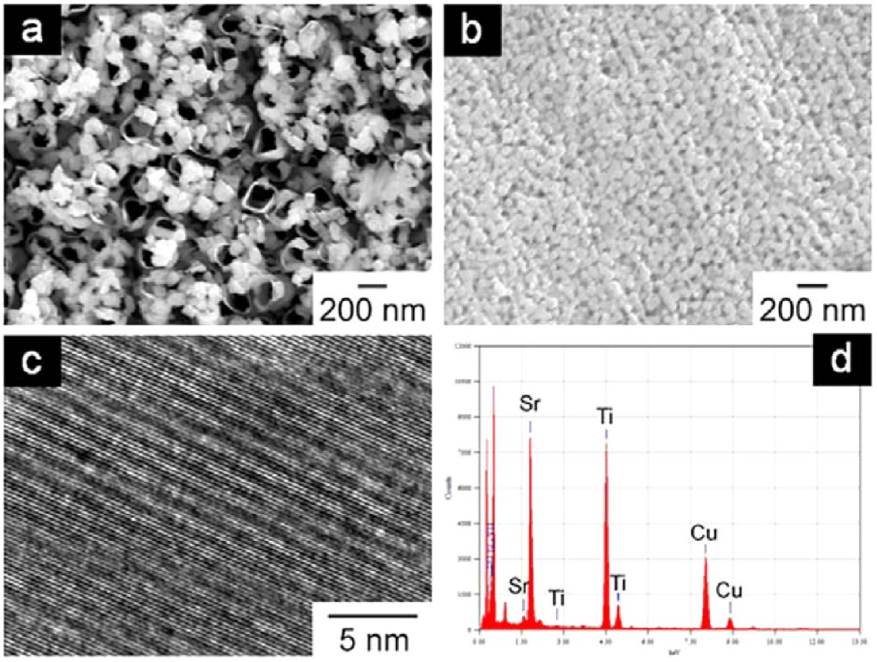

Figure 4. SEM images of $SrTiO_3$−TiO_2 nanoparticle−nanotube heterostructures: (a) 1.4-Sr/TNTs and (b) 6.3-Sr/TNTs; (c) high resolution TEM image of $SrTiO_3$ nanoparticles in 6.3-Sr/TNTs; and (d) EDX analysis of 6.3-Sr/TNTs.

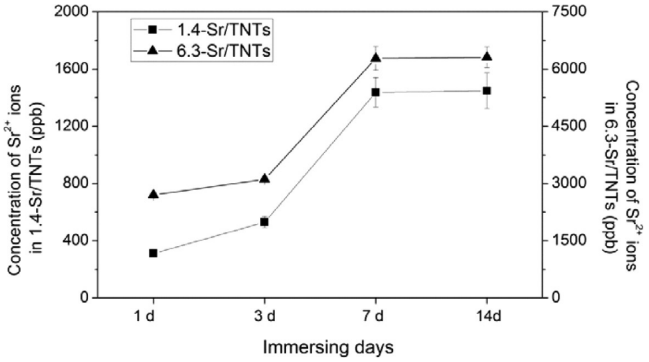

Figure 5. Concentrations of Sr^{2+} ions in cell culture media released from 1.4-Sr/TNTs and 6.3-Sr/TNTNs after immersing in cell media solution for 1 d, 3 d, 7 d, and 14 d.

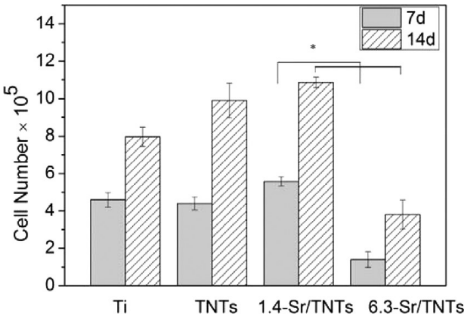

Figure 6. Cell numbers on Ti, TNTs, 1.4-Sr/TNTs, and 6.3-Sr/TNTs.

ordered arrays. Similar heterostructures with improved photoelectrochemical performance were reported by Zhang et al.[11] and Jiao et al.[12]

As shown in the XRD pattern (Figure 1c), $SrTiO_3$ was synthesized through hydrothermal reactions for 12 h, though $SrTiO_3$ was not detected for the short hydrothermal reaction time of 3 h due to the low volume fraction. The reaction mechanism of $SrTiO_3$ is a transformation from titanium dioxide to titanate, given by[25]

$$TiO_2 + Sr(OH)_2 \rightarrow SrTiO_3 + H_2O \quad (3)$$

It was reported that TiO_2 with anatase structure is stable in a solution of pH value greater than 2, and the total molality ($m_{Ti,T}$) of the titanium species was greater than 10^{-7}.[26] In this study, the stable species was $Ti(OH)_4$ (aqueous).

The $Sr(OH)_2$ was ionized to Sr^{2+} and OH^- ions during the hydrothermal process in an aqueous solution, given by

$$Sr(OH)_2 \rightarrow Sr^{2+} + 2OH^- \quad (4)$$

In the hydrothermal process, Sr did not substitute Ti directly. The hydrothermal process could be described as follows. At the early stage of the hydrothermal process, TiO_2 was dissolved in water and formed $Ti(OH)_4$ given by

$$TiO_2 + 2H_2O \rightarrow Ti(OH)_4 \quad (5)$$

The $Ti(OH)_4$ then combined with the OH^- ions and formed $[Ti(OH)_6]^{2-}$:

$$Ti(OH)_4 + 2OH^- \rightarrow [Ti(OH)_6]^{2-} \quad (6)$$

Subsequently, $[Ti(OH)_6]^{2-}$ reacted with Sr^{2+} ions and formed $SrTiO_3$ nanoparticles on the surface of TNTs given by

$$[Ti(OH)_6]^{2-} + Sr^{2+} \rightarrow SrTiO_3 + 3H_2O \quad (7)$$

With the progress of the hydrothermal process, $SrTiO_3$ nanoparticles formed and deposited on the walls of TiO_2 nanotubes, leading to a nanoparticle−nanotube heterostructure, as shown in Figure 9. As the time of the hydrothermal process increased, the synthesis of the $SrTiO_3$ nanoparticles was controlled by the in situ hydrolysis of the TNTs.

The hydrolysis of TiO_2 nanotubes started from the grain boundaries between the TiO_2 crystals. Thus, the thickness of the walls of the nanotubes became thin, and the TiO_2 crystals became separated from each other with increasing hydro-

DOI: 10.1021/acsami.5b04304
ACS Appl. Mater. Interfaces 2015, 7, 16018−16026

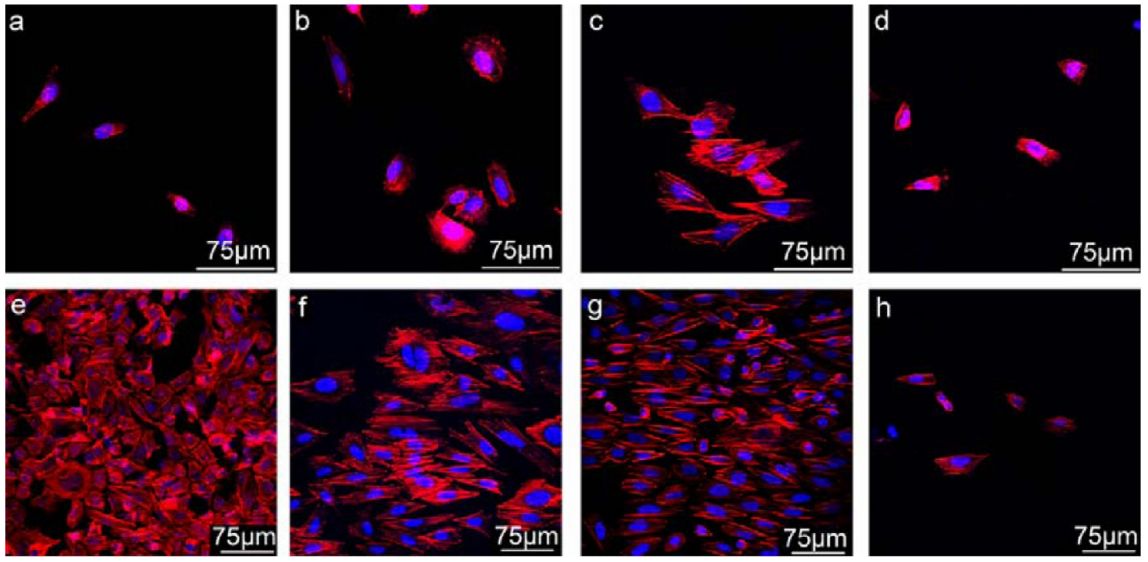

Figure 7. Morphologies of SaOS2 cells observed by confocal microscopy: (a and e) on Ti, (b and f) on TNTs, (c and g) on 1.4-Sr/TNTs, and (d and h) on 6.3-Sr/TNTs after cell culture for 1 and 5 d, respectively.

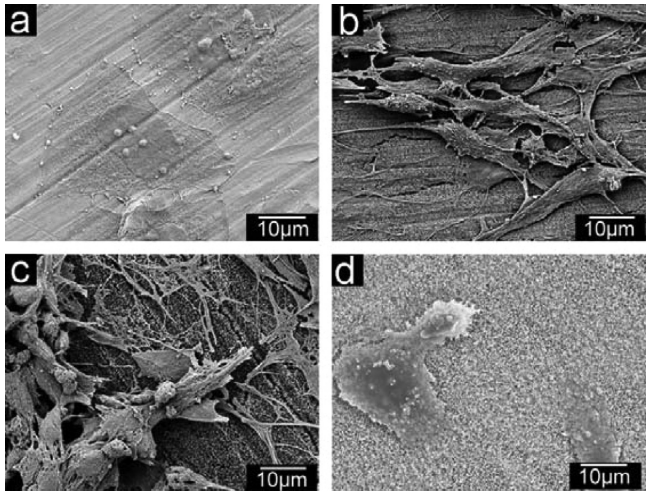

Figure 8. SEM images of morphologies of SaOS2 cells on: (a) Ti, (b) TNTs, (c) 1.4-Sr/TNTs, and (d) 6.3-Sr/TNTs after cell culture for 5 d.

thermal time (as shown in Figure 10). The TiO_2 nanotubes collapsed with the growth of the $SrTiO_3$ nanoparticles. The number of $SrTiO_3$ nanoparticles on the surface of the TNTs increased with the increasing of the reaction time.

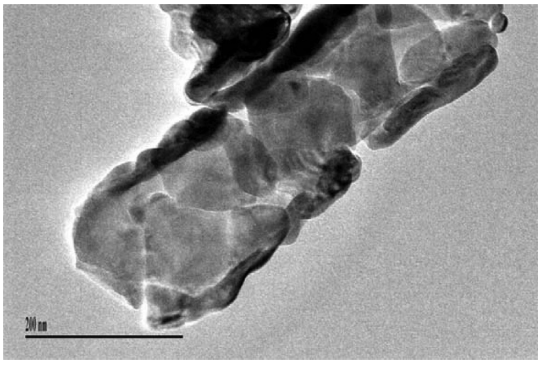

Figure 10. TEM morphology of the hydrolytic TiO_2 nanotubes.

The Sr/TNTs nanoparticle−nanotube heterostructures showed considerable release of Sr^{2+} ions during cell culture media immersion (Figure 5). The hydrolysis process of $SrTiO_3$ nanoparticles was similar to that of other titanates, such as $BaTiO_3$.[27] The release of Sr^{2+} ions from Sr/TNTs could be described as follows:

$$SrTiO_3 + H_2O \rightarrow Sr^{2+} + TiO_2 + 2OH^- \quad (8)$$

The concentration of Sr^{2+} ions released from 6.3-Sr/TNTs was nine times higher than that from 1.4-Sr/TNTs after 1 d

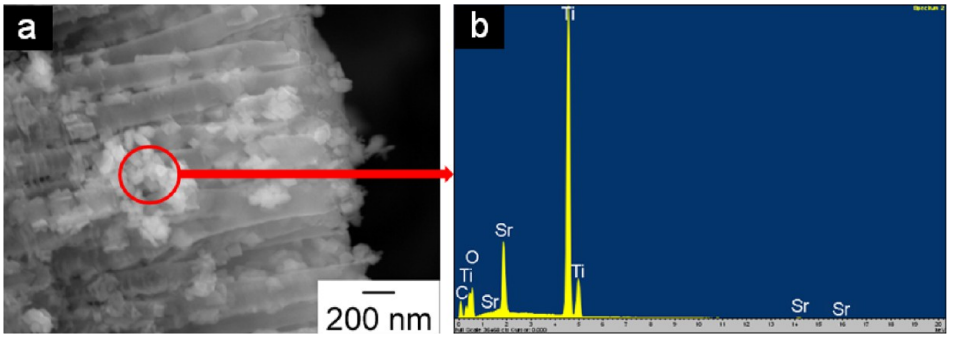

Figure 9. (a) Cross-sectional view of 1.4-Sr/TNTs nanoparticle−nanotube heterostructures; (b) EDX spectra of the $SrTiO_3$ nanoparticles.

DOI: 10.1021/acsami.5b04304
ACS Appl. Mater. Interfaces 2015, 7, 16018−16026

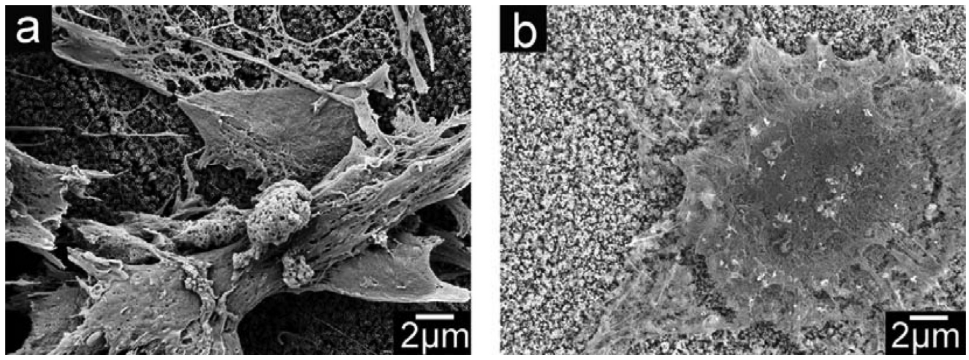

Figure 11. High magnification SEM images of morphologies of SaOS2 cells after cell culture for 5 d: (a) 1.4-Sr/TNTs and (b) 6.3-Sr/TNTs.

immersing in cell culture media (Figure 5). After 7 and 14 d immersing, the Sr^{2+} concentration of 6.3-Sr/TNTs was 4.3 times higher than that from 1.4-Sr/TNTs. The higher volume fraction of $SrTiO_3$ nanoparticles in 6.3-Sr/TNTs resulted in a higher released concentration of Sr^{2+} ions in cell culture media than that for 1.4-Sr/TNTs. The maximum concentration of Sr^{2+} ions for 1.4-Sr/TNTs was 1448 ppb after immersing 14 d. In contrast, the concentrations of Sr^{2+} ions released from 6.3-Sr/TNTs were 2700 and 6282 ppb after 1 and 14 d immersing, respectively.

The $SrTiO_3$−TiO_2 heterostructures exhibited comparable release ability of Sr^{2+} ions to apatite based biocements.[18,28] Sr modified cements released 300−700 ppb Sr^{2+} ions in cell culture media after immersing for 21 d.[18] The concentration of Sr^{2+} ions released from Sr-substituted hydroxyapatite coatings was 1000 ppb in SBF solution.[28] Sr-apatite cement released Sr^{2+} ions with a concentration of 4000 ppb after immersing 14 d in water.[29]

4.2. Effect of strontium on biocompatibility. Strontium has been reported to possess the ability to stimulate new bone formation and inhibit the resorption of osteoclast cells.[30,31] The beneficial effect of stimulating new bone formation for the low concentration of strontium ions was evidenced by the cell proliferation result of 1.4-Sr/TNTs after cell culture for 7 and 14 d (Figure 6). The cell attachment and spreading observed by using confocal microscopy also indicated less SaOS2 cells on 6.3-Sr/TNTs than on 1.4-Sr/TNTs.

Previous studies also demonstrated the beneficial effect of a low concentration of Sr ions in stimulating new bone formation.[30,32−34] The proliferation of osteoblast cells was significantly enhanced with Sr added to hardystonite ceramic coatings.[35] In this study, the proliferation of cells showed that the release of Sr ions in 1.4-Sr/TNTs was suitable for stimulating the proliferation of SaOS2 cells. The higher release of Sr ions from 6.3-Sr/TNTs inhibited the proliferation of SaOS2 cells. There was an optimum addition of Sr observed in a previous study.[36] The morphology observation for the SaOS2 cells demonstrated that the adhesion and spreading of SaOS2 cells were inhibited on the surface of 6.3-Sr/TNTs.

The inhibitory effect of a high concentration of Sr ions was exerted by suppressing the differentiation and proliferation of osteoclast cells.[34,37] It was reported that the differentiation of osteoclast cells (RAW264.7) was suppressed when the concentration of Sr was higher than 38.7 at % in the hydroxyapatite coatings.[34] In another study,[37] HA films with Sr concentration higher than 3 at % showed increased osteoprotegerin to activation-induced cytokine receptor ratio, which is an indicator of deterioration of osteoclastic activities.

A high dose of Sr has been demonstrated to have a deleterious effect on biocompatibility, and a suitable dose was closely related to the delivery system and cell lineage.[18,32,38] Sr^{2+} ions released from strontium ranelate with concentration of 0.5 mM demonstrated stronger influence on the proliferation and ALP activities of osteoblastic cells than even higher concentration of Sr^{2+} ions.[38] The maximum concentration of Sr in calcium phosphate bone cements was 0.1 mM, and the adverse effect of Sr was observed with even higher concentration.[18] With 5 at % Sr substitution of Ca in biphasic calcium phosphate, the protein activity and cell proliferation showed better performance than with higher Sr substitution.[32] 1 mM and higher $SrCl_2$ inhibited the regeneration and bioactivity of cells.[32]

Overall, the concentration of Sr in $SrTiO_3$−TiO_2 heterostructures was one of the factors determining the biological performance. Higher concentration of Sr, that is, >3000 ppb, inhibited the proliferation of SaOS2 cells.

4.3. Adhesion and spreading of SaOS2 cells on Sr/TNTs. In this study, samples with TiO_2 nanotubular topography significantly promoted the secretion of extracellular matrix components and the growth of filopodia. Dense cytoskeletons were developed to anchor the surface of substrate after culturing cells for 1 d on 1.4-Sr/TNTs (Figure 7c).

The topographies of implant surfaces determined the attachment and spreading of osteoblasts cells.[39,40] TNTs demonstrated different nanotopography after hydrothermal reactions with $Sr(OH)_2$. 1.4-Sr/TNTs consisted of TiO_2 nanotubes decorated with $SrTiO_3$ nanoparticles, while 6.3-Sr/TNTs was a full layer of $SrTiO_3$ nanoparticles with a size of about 50 nm. The roughness, surface energy, and wettability of samples were also changed after hydrothermal processing (as shown in Figure 4 and Table 1). Biomaterials with nanoscale topography could stimulate cells to secrete abundant fibril-type extracellular matrix materials.[39] As shown in the confocal images (Figure 7), cells exhibited significant morphological difference on TNTs and 1.4-Sr/TNTs compared with bare Ti and 6.3-Sr/TNTs. Cells on TNTs and 1.4-Sr/TNTs spread numerous cytoskeletons, binding tightly with the substrate and interconnecting with contiguous cells. Osteoblast cells attached randomly on the surface of bare Ti without any obvious alignment caused by the surface. The cytoskeletons of SaOS2 cells on TNTs[42] and 1.4-Sr/TNTs exhibited an organized shape, which was also a mark for the high mobility of cells.

Cells showed a rounder shape on 6.3-Sr/TNTs than on 1.4-Sr/TNTs (as shown in Figure 8c and 8d). Actin cytoskeletons are essential for the maintenance of cell shape and the attachment of cells to implants. One of the possible reasons for

DOI: 10.1021/acsami.5b04304
ACS Appl. Mater. Interfaces 2015, 7, 16018−16026

the elongated cellular shape was that the development of cytoskeletons which connected cells with the surface was influenced by the morphology of nanotubes. There were more lateral points available for long filopodia to bind with the implants through cell integrin to acquire a firm contact. In addition, the sharp and vertical walls of TiO_2 nanotubes had an ability to trigger the development and spreading of filopodia.[41] In 6.3-Sr/TNTs samples, the $SrTiO_3$ nanoparticles filled and covered the TiO_2 nanotubes; therefore, focal contacts were established between cells and substrates without elongated filopodia.[41] Thus, the osteoblast cells grew a round shape on the surface of 6.3-Sr/TNTs, indicating an unhealthy status.

The enhanced interconnection between SaOS2 cells on TNTs and 1.4-Sr/TNTs was shown in Figure 11. The TiO_2 nanotubes showed a positive influence in inducing secretion and organization of filopodia compared with bare Ti. The bare Ti samples lacked nanostructure topography to signal the development of extracellular matrix fibril. As shown in Figure 7 and Figure 8, longer filopodia were observed on the surface of TNTs and 1.4-Sr/TNTs than that on bare Ti and 6.3-Sr/TNTs. Osteoblast cells interconnected with each other well through production of fibrils.

The adhesion of osteoblast cells on the implants was established in two steps. First, electrostatic forces connected the cell membrane and implants through a nonspecific contact.[44] In the second step, a specific and focal binding was established through integrin between cells and implants.[43] Therefore, abundant filopodia in the layer of TNTs and 1.4-Sr/TNTs supported the attachment and spreading of cells. The integrins of cell membrane exhibited preference to a curved surface with sharp edges.[45] 1.4-Sr/TNTs exhibited a sharper and much more curved topography than 6.3-Sr/TNTs. The increased attachment of cells was one of the reasons for the enhanced cell proliferation for 1.4-Sr/TNTs.

The surface layer of 6.3-Sr/TNTs had an adverse influence on the development extracellular matrix production. In contrast, 1.4-Sr/TNTs showed a positive effect in stimulating the proliferation and attachment of SaOS2 cells.

4.4. Effect of surface energy and hydrophilicity on biocompatibility. The surface roughness of Ti, TNTs, 1.4-Sr/TNTs, and 6.3-Sr/TNTs was not significantly different, as shown in Figure 2. However, the surface energy was significantly changed after introducing the TNTs and $SrTiO_3$ decorated TNTs with different volume fractions of $SrTiO_3$ particles on the surface (Table 1). It has been reported that the surface energy and hydrophilicity would affect the biocompatibility positively through changing the absorption ability of the surface.[46] In this study, the surface energy of 1.4-Sr/TNTs was the highest (65.60 mJ/m^2) among the four kinds of surfaces and the surface energy of Ti was the lowest (26.78 mJ/m^2), while the TNTs showed a higher surface energy (55.53 mJ/m^2) than that of 6.3-Sr/TNTs (41.59 mJ/m^2). The highest surface energy of 1.4-Sr/TNTs is probably due to its unique surface chemistry of $SrTiO_3$−TiO_2 and the special topography of nanoparticle decorated on nanotubes. The difference between the surface roughness of 6.3-Sr/TNTs and 1.4-Sr/TNTs is not significant, as 88.7 and 75.9 nm. It has been indicated that high surface energy is beneficial to the growth of cells on implants.[46] In the cell culture media, surfaces with higher surface energy are assumed to possess an advantage to absorb the anions and organic hydrocarbon molecules from the media.[47]

In a similar way, 1.4-Sr/TNTs showed the highest hydrophilicity and the pure Ti showed the lowest, while the TNTs showed a higher hydrophilicity than that of 6.3-Sr/TNTs, as shown in Figure 3. The high hydrophilicity of the 1.4-Sr/TNTs surface may lead to enhanced absorption of molecules from the cell culture media. Buser et al.[48] indicated that surface hydrophilicity might stimulate bone mineralization and osteointegration. The main phase of 1.4-Sr/TNTs was still the highly hydrophilic TNTs of anatase TiO_2; therefore, the surface of 1.4-Sr/TNTs showed the highest cell proliferation among the four kinds of surfaces (Figure 6).

The surface of 1.4-Sr/TNTs exhibited a nanoparticle−nanotube heterostructure, while the surface of 6.3-Sr/TNTs was covered by a nearly uniform layer of nanoparticles of $SrTiO_3$. It can be deduced that the adsorption ability of the 1.4-Sr/TNTs was enhanced due to the nanotubular topography of the heterostructure.[6] Thus, 1.4-Sr/TNTs exhibited better biocompatibility compared to the surfaces of Ti, TNTs, and 6.3-Sr/TNTs due to the preferable surface environment for SaOS2 cells to attach and spread.

5. CONCLUSIONS

$SrTiO_3$−TiO_2 nanoparticle−nanotube heterostructures were fabricated via anodization combined with hydrothermal processing for biomedical applications. The volume fraction of the $SrTiO_3$ nanoparticles (in other words, the concentration of Sr) in the heterostructures was controlled through adjusting the hydrothermal reaction time. The hydrophilicity of the $SrTiO_3$−TiO_2 heterostructures decreased with increasing the volume fraction of $SrTiO_3$ in the heterostructure. The release of Sr^{2+} ions from $SrTiO_3$−TiO_2 reached a stable state after immersing in cell culture media for 7 d. The TiO_2 nanotubes and the $SrTiO_3$−TiO_2 heterostructures with low Sr concentration exhibited significantly enhanced cell proliferation compared with bare Ti, while $SrTiO_3$−TiO_2 with high Sr concentration showed inhibited cell proliferation and limited spreading of SaOS2 cells. A greater number of longer filopodia of SaOS2 cells were observed on the surface of $SrTiO_3$−TiO_2 with low Sr concentration, compared to bare Ti, TiO_2 nanotubes, and $SrTiO_3$−TiO_2 with high Sr concentration, indicating a superior biocompatibility of the low Sr concentration $SrTiO_3$−TiO_2 heterostructure. Our results indicated that the optimum Sr^{2+} ion release from a $SrTiO_3$−TiO_2 heterostructure is 1.4 ppm, while a Sr^{2+} ion release ≥3.0 ppm would inflict an adverse effect on SaOS2 cells.

AUTHOR INFORMATION

Corresponding Author

*Tel.: +61399257560. Fax: +61399256108. E-mail: yuncang.li@rmit.edu.au.

Notes

The authors declare no competing financial interest.

ACKNOWLEDGMENTS

The authors are grateful to Paul Morrison, School of Applied Sciences, RMIT University, for his technical support in the ion concentration analysis using ICP-MS. C.W. and Y.L. acknowledge the support for this research by NHMRC through Grant GNT1087290.

REFERENCES

(1) Niinomi, M. Recent Metallic Materials for Biomedical Applications. *Metall. Mater. Trans. A* **2002**, *33*, 477−486.

DOI: 10.1021/acsami.5b04304
ACS Appl. Mater. Interfaces 2015, 7, 16018−16026

(2) Long, M.; Rack, H. J. Titanium Alloys in Total Joint Replacement—A Materials Science Perspective. *Biomaterials* **1998**, *19*, 1621−1639.
(3) Williams, D. F. On the Mechanisms of Biocompatibility. *Biomaterials* **2008**, *29*, 2941−2953.
(4) Davies, J. E. Understanding Peri-implant Endosseous Healing. *J. Dent. Educ.* **2003**, *67*, 932−949.
(5) Liu, X.; Chu, P. K.; Ding, C. Surface Nano-functionalization of Biomaterials. *Mater. Sci. Eng., R* **2010**, *70*, 275−302.
(6) Roy, P.; Berger, S.; Schmuki, P. TiO_2 Nanotubes: Synthesis and Applications. *Angew. Chem., Int. Ed.* **2011**, *50*, 2904−2939.
(7) Shrestha, N. K.; Macak, J. M.; Schmidt-Stein, F.; Hahn, R.; Mierke, C. T.; Fabry, B.; Schmuki, P. Magnetically Guided Titania Nanotubes for Site-Selective Photocatalysis and Drug Release. *Angew. Chem.* **2009**, *121*, 987−990.
(8) Schmidt-Stein, F.; Hahn, R.; Gnichwitz, J.-F.; Song, Y. Y.; Shrestha, N. K.; Hirsch, A.; Schmuki, P. X-ray Induced Photocatalysis on TiO_2 and TiO_2 Nanotubes: Degradation of Organics and Drug Release. *Electrochem. Commun.* **2009**, *11*, 2077−2080.
(9) Song, Y.; Schmidt-Stein, F.; Bauer, S.; Schmuki, P. Amphiphilic TiO2 Nanotube Arrays: An Actively Controllable Drug Delivery System. *J. Am. Chem. Soc.* **2009**, *131*, 4230−4232.
(10) Popat, K. C.; Eltgroth, M.; LaTempa, T. J.; Grimes, C. A.; Desai, T. A. Titania Nanotubes: A Novel Platform for Drug-Eluting Coatings for Medical Implants. *Small* **2007**, *3*, 1878−1881.
(11) Zhang, J.; Bang, J. H.; Tang, C.; Kamat, P. V. Tailored TiO_2-$SrTiO_3$ Heterostructure Nanotube Arrays for Improved Photoelectrochemical Performance. *ACS Nano* **2010**, *4*, 387−395.
(12) Jiao, Z.; Zhang, Y.; Chen, T.; Dong, Q.; Lu, G.; Bi, Y. TiO_2 Nanotube Arrays Modified with Cr-Doped $SrTiO_3$ Nanocubes for Highly Efficient Hydrogen Evolution under Visible Light. *Chem. - Eur. J.* **2014**, *20*, 2654−2662.
(13) Xin, Y.; Jiang, J.; Huo, K.; Hu, T.; Chu, P. K. Bioactive $SrTiO_3$ Nanotube Arrays: Strontium Delivery Platform on Ti-Based Osteoporotic Bone Implants. *ACS Nano* **2009**, *3*, 3228−3234.
(14) Zhao, L.; Wang, H.; Huo, K.; Zhang, X.; Wang, W.; Zhang, Y.; Wu, Z.; Chu, P. K. The Osteogenic Activity of Strontium Loaded Titania Nanotube Arrays on Titanium Substrates. *Biomaterials* **2013**, *34*, 19−29.
(15) Guin, D.; Manorama, S. V.; Latha, J. N. L.; Singh, S. Photoreduction of Silver on Bare and Colloidal TiO_2 Nanoparticles/Nanotubes: Synthesis, Characterization, and Tested for Antibacterial Outcome. *J. Phys. Chem. C* **2007**, *111*, 13393−13397.
(16) Cheng, H.; Li, Y.; Huo, K.; Gao, B.; Xiong, W. Long-lasting in vivo and in vitro Antibacterial abiliTy of Nanostructured Titania Coating Incorporated with Silver Nanoparticles. *J. Biomed. Mater. Res., Part A* **2014**, *102*, 3488−3499.
(17) Zhang, W.; Shen, Y.; Pan, H.; Lin, K.; Liu, X.; Darvell, B. W.; Lu, W. W.; Chang, J.; Deng, L.; Wang, D.; Huang, W. Effects of Strontium in Modified Biomaterials. *Acta Biomater.* **2011**, *7*, 800−808.
(18) Schumacher, M.; Lode, A.; Helth, A.; Gelinsky, M. A Novel Strontium(II)-modified Calcium Phosphate Bone Cement Stimulates Human-Bone-Marrow-Derived Mesenchymal Stem Cell Proliferation and Osteogenic Differentiation in vitro. *Acta Biomater.* **2013**, *9*, 9547−9557.
(19) Park, J.-W.; Kim, H.-K.; Kim, Y.-J.; Jang, J.-H.; Song, H.; Hanawa, T. Osteoblast Response and Osseointegration of a Ti−6Al−4V Alloy Implant Incorporating Strontium. *Acta Biomater.* **2010**, *6*, 2843−2851.
(20) Dahl, S. G.; Allain, P.; Marie, P. J.; Mauras, Y.; Boivin, G.; Ammann, P.; Tsouderos, Y.; Delmas, P. D.; Christiansen, C. Incorporation and Distribution of Strontium in Bone. *Bone* **2001**, *28*, 446−453.
(21) Fu, Y.; Chen, D. Influence of Sr^{2+} on Strontium Substitued Hydroxyapatite's (Sr-HA) Cytotoxicity. *J. Oral Tissue Engin.* **2005**, *2*, 76−80.
(22) Wang, Y.; Wen, C.; Hodgson, P.; Li, Y. Biocompatibility of TiO_2 Nanotubes with Different Topographies. J. *J. Biomed. Mater. Res., Part A* **2014**, *102*, 743−751.
(23) Owens, D. K.; Wendt, R. C. Estimation of the Surface Free Energy of Polymers. *J. Appl. Polym. Sci.* **1969**, *13*, 1741−1747.
(24) Carré, A. Polar Interactions at Liquid/Polymer Interfaces. *J. Adhes. Sci. Technol.* **2007**, *21*, 961−981.
(25) Eckert, J. O.; Hung-Houston, C. C.; Gersten, B. L.; Lencka, M. M.; Riman, R. E. Kinetics and Mechanisms of Hydrothermal Synthesis of Barium Titanate. *J. Am. Ceram. Soc.* **1996**, *79*, 2929−2939.
(26) Lencka, M. M.; Riman, R. E. Thermodynamics of the Hydrothermal Synthesis of Calcium Titanate with Reference to Other Alkaline-Earth Titanates. *Chem. Mater.* **1995**, *7*, 18−25.
(27) Blanco López, M. C.; Rand, B.; Riley, F. L. The Tsoelectric Point of $BaTiO_3$. *J. Eur. Ceram. Soc.* **2000**, *20*, 107−118.
(28) Yin, P.; Feng, F. F.; Lei, T.; Zhong, X. H.; Jian, X. C. Osteoblastic Cell Response on Biphasic Fluorhydroxyapatite/Strontium-Substituted Hydroxyapatite Coatings. *J. Biomed. Mater. Res., Part A* **2014**, *102*, 621−627.
(29) Sekine, K.; Sakama, M.; Hamada, K. In Evaluation of Strontium Introduced Apatite Cement as the Injectable Bone Substitute Developments. *Eng. Med. Biol. Soc. (EMBC), 35th Annu. Int. Conf.* IEEE: 2013; pp 858−861.
(30) Meunier, P. J.; Roux, C.; Seeman, E.; Ortolani, S.; Badurski, J. E.; Spector, T. D.; Cannata, J.; Balogh, A.; Lemmel, E.-M.; Pors-Nielsen, S.; Rizzoli, R.; Genant, H. K.; Reginster, J.-Y. The Effects of Strontium Ranelate on the Risk of Vertebral Fracture in Women with Postmenopausal Osteoporosis. *N. Engl. J. Med.* **2004**, *350*, 459−468.
(31) Pors Nielsen, S. The Biological Role of Strontium. *Bone* **2004**, *35*, 583−588.
(32) Braux, J.; Velard, F.; Guillaume, C.; Bouthors, S.; Jallot, E.; Nedelec, J.-M.; Laurent-Maquin, D.; Laquerrière, P. A New Insight into the Dissociating Effect of Strontium on Bone Resorption and Formation. *Acta Biomater.* **2011**, *7*, 2593−2603.
(33) Ni, G. X.; Shu, B.; Huang, G.; Lu, W. W.; Pan, H.-B. The Effect of Strontium Incorporation into Hydroxyapatites on their Physical and Biological Properties. *J. Biomed. Mater. Res., Part B* **2012**, *100B*, 562−568.
(34) Chung, C. J.; Long, H. Y. Systematic Strontium Substitution in Hydroxyapatite Coatings on Titanium via Micro-arc Treatment and their Osteoblast/osteoclast Responses. *Acta Biomater.* **2011**, *7*, 4081−4087.
(35) Zhang, W.; Wang, G.; Liu, Y.; Zhao, X.; Zou, D.; Zhu, C.; Jin, Y.; Huang, Q.; Sun, J.; Liu, X.; Jiang, X.; Zreiqat, H. The Synergistic Effect of Hierarchical Micro/nano-topography and Bioactive Ions for Enhanced Osseointegration. *Biomaterials* **2013**, *34*, 3184−3195.
(36) Yin, P.; Feng, F. F.; Lei, T.; Zhong, X. H.; Jian, X. C. Osteoblastic Cell Response on Biphasic Fluorhydroxyapatite/strontium-substituted Hydroxyapatite Coatings. *J. Biomed. Mater. Res., Part A* **2014**, *102*, 621−7.
(37) Capuccini, C.; Torricelli, P.; Sima, F.; Boanini, E.; Ristoscu, C.; Bracci, B.; Socol, G.; Fini, M.; Mihailescu, I. N.; Bigi, A. Strontium-substituted Hydroxyapatite Coatings Synthesized by Pulsed-laser Deposition: In vitro Osteoblast and Osteoclast Response. *Acta Biomater.* **2008**, *4*, 1885−1893.
(38) Barbara, A.; Delannoy, P.; Denis, B. G.; Marie, P. J. Normal Matrix Mineralization Induced by Strontium Ranelate in MC3T3-E1 Osteogenic Cells. *Metab., Clin. Exp.* **2004**, *53*, 532−537.
(39) von der Mark, K.; Park, J.; Bauer, S.; Schmuki, P. Nanoscale Engineering of Biomimetic Surfaces: Cues from the Extracellular Matrix. *Cell Tissue Res.* **2010**, *339*, 131−153.
(40) Liu, X.; Chu, P. K.; Ding, C. Surface Modification of Titanium, Titanium Alloys, and Related Materials for Biomedical Applications. *Mater. Sci. Eng., R* **2004**, *47*, 49−121.
(41) Brammer, K. S.; Oh, S.; Frandsen, C. J.; Varghese, S.; Jin, S. Nanotube Surface Triggers Increased Chondrocyte Extracellular Matrix Production. *Mater. Sci. Eng., C* **2010**, *30*, 518−525.
(42) Narayanan, R.; Lee, H.-J.; Kwon, T.-Y.; Kim, K.-H. Anodic TiO_2 Nanotubes from Stirred Baths: Hydroxyapatite Growth & Osteoblast Responses. *Mater. Chem. Phys.* **2011**, *125*, 510−517.

DOI: 10.1021/acsami.5b04304
ACS Appl. Mater. Interfaces 2015, 7, 16018−16026

(43) Ohara, P. T.; Buck, R. C. Contact Guidance in vitro: A light, Transmission, and Scanning Electron Microscopic study. *Exp. Cell Res.* **1979**, *121*, 235−249.
(44) Kabaso, D.; Gongadze, E.; Perutková, Š.; Matschegewski, C.; Kralj-Iglič, V.; Beck, U.; van Rienen, U.; Iglič, A. Mechanics and Electrostatics of the Interactions between Osteoblasts and Titanium Surface. *Comput. Methods Biomech. Biomed. Eng.* **2011**, *14*, 469−482.
(45) Iglič, A.; Gongadze, E.; K, D.; Bauer, S.; Slivnik, T.; Schmuki, P. P.; van Rienen, U. Adhesion of Osteoblasts to A Nanorough Titanium Implant Surface. *Int. J. Nanomed.* **2011**, *6*, 1801−1816.
(46) Zhao, G.; Schwartz, Z.; Wieland, M.; Rupp, F.; Geis-Gerstorfer, J.; Cochran, D. L.; Boyan, B. D. High Surface Energy Enhances Cell Response to Titanium Substrate Microstructure. *J. Biomed. Mater. Res., Part A* **2005**, *74A*, 49−58.
(47) Textor, M.; Sittig, C.; Frauchiger, V.; Tosatti, S.; Brunette, D. Properties and Biological Significance of Natural Oxide Films on Titanium and Its Alloys. In *Titanium in Medicine*; Springer: Berlin Heidelberg, 2001; pp 171−230.
(48) Buser, D.; Broggini, N.; Wieland, M.; Schenk, R. K.; Denzer, A. J.; Cochran, D. L.; Hoffmann, B.; Lussi, A.; Steinemann, S. G. Enhanced Bone Apposition to a Chemically Modified SLA Titanium Surface. *J. Dent. Res.* **2004**, *83*, 529−533.

DOI: 10.1021/acsami.5b04304
ACS Appl. Mater. Interfaces 2015, 7, 16018−16026